J|A|C|S ARTICLES

Published on Web 03/04/2009

Experimental and Theoretical Analysis of Asymmetric Induction in Heterogeneous Catalysis: Diastereoselective Hydrogenation of Chiral α-Hydroxyketones over Pt Catalyst

Igor Busygin,[†,||] Antti Taskinen,[‡] Ville Nieminen,[‡] Esa Toukoniitty,[‡] Thomas Stillger,[§] Reko Leino,*[,†] and Dmitry Yu. Murzin*[,‡]

Laboratory of Organic Chemistry and Laboratory of Industrial Chemistry and Reaction Engineering, Åbo Akademi University, FI-20500 Turku/Åbo, Finland, and Faculty of Chemistry, Pharmacy, and Earth Sciences, University of Freiburg, Hebelstraβe 27, D-79085 Freiburg, Germany

Received November 20, 2008; E-mail: rleino@abo.fi; dmurzin@abo.fi

Abstract: Assessing the origin of asymmetric induction in heterogeneously catalyzed hydrogenation is a challenging task. In this work, hydrogenation of a chiral compound, (*R*)-1-hydroxy-1-phenyl-2-propanone [(*R*)-PAC], in toluene over cinchonidine modified and unmodified Pt/Al_2O_3 was studied. To reveal the detailed reaction mechanism and the origin of stereoselectivity in the Pt-catalyzed hydrogenation of the C═O double bond, the structures and energies of several adsorption modes of (*R*)-PAC as well as whole reaction paths for hydrogenation were investigated on Pt(111) by density functional theory (DFT). In agreement with experimental results, the theoretically obtained potential energy profiles for the studied hydrogenation mechanisms implied that (1*R*,2*S*)-1-phenyl-1,2-propanediol is formed in excess with respect to the other diastereomeric product diol, (1*R*,2*R*)-1-phenyl-1,2-propanediol. Generally, if the elementary hydrogen addition step was thermodynamically more favorable on one of the two diastereotopic faces, it was also kinetically preferred on the same face, and vice versa. Pairwise addition of hydrogen was the most energetically favorable mechanism. Adsorption and hydrogenation of other structurally similar chiral α-hydroxyketones, (*R*)-3-hydroxy-2-butanone and (*R*)-2-hydroxy-1-cyclohexanone, were also studied computationally on Pt(111). The results showed that cluster model DFT calculations can be used to assess (dia)stereoselectivity in metal-catalyzed hydrogenation of even such complex organic molecules as studied here.

1. Introduction

Various asymmetric synthetic methods have been applied to produce optically active organic molecules required by the increasing demand from the pharmaceutical and fine chemical industries. Hydrogenation of prochiral C═C, C═O, and C═N functionalities is one of the most useful tools to create asymmetry in a molecule. In the reduction of prochiral C═X moieties, racemic mixtures are obtained unless the reaction is carried out in a chiral environment. In laboratory practice, various sources of asymmetric induction can be utilized, including chiral reducing agents, chiral solvents, and transition metal complexes with chiral ligands in homogeneous phase; chirally modified metal catalysts and chiral metal complexes immobilized on the surface of a heterogeneous matrix; and enzymes.

An alternative to the classical strategies is to use substrates that are the source of chirality themselves and that thereby can influence the configuration of a newly formed stereogenic center. This methodology is widely adopted for some homogeneously catalyzed reactions,[1] while there are only a few literature reports showing mediocre to good diastereomeric excesses (de) when a chiral substrate is subjected to a reaction over a heterogeneous surface. However, as compared to the homogeneous catalysts, heterogeneous counterparts have many advantages such as easy separation, feasible recovery and recycling, simple handling, good stability, and availability, which are important in industrial production. The aforementioned diastereoselective approach has been applied to heterogeneous catalytic hydrogenation of prochiral C═C bonds, for example, in the hydrogenation of racemic Baylis−Hillman adducts over Pd and Ni catalysts.[2] The diastereoselective hydrogenation of Schiff bases obtained by the condensation of optically active amines and prochiral ketones is a widely utilized strategy for chiral compounds.[3] Hydrogenation of substituted aromatic rings such as pyridines[4] and benzenes[5] has also been performed with high diastereoselectivities. Surprisingly, the diastereoselective heterogeneous cata-

[†] Laboratory of Organic Chemistry, Åbo Akademi University.
[‡] Laboratory of Industrial Chemistry and Reaction Engineering, Åbo Akademi University.
[§] University of Freiburg.
[||] Current address: CAT Catalytic Center, ITMC, RWTH Aachen University, Worringerweg 1, D-52074 Aachen, Germany.

(1) Hoveyda, A. H.; Evans, D. A.; Fu, G. C. *Chem. Rev.* **1993**, *93*, 1307.
(2) (a) Mateus, C. R.; Almeida, W. P.; Coelho, F. *Tetrahedron Lett.* **2000**, *41*, 2533. (b) Mateus, C. R.; Feltrin, M. P.; Costa, A. M.; Coelho, F.; Almeida, W. P. *Tetrahedron* **2001**, *57*, 6901. (c) Saxena, R.; Singh, V.; Batra, S. *Tetrahedron* **2004**, *60*, 10311.
(3) See, for example: (a) Nugent, T. C.; Ghosh, A. K.; Wakchaure, V. N.; Mohanty, R. R. *Adv. Synth. Catal.* **2006**, *348*, 1289. (b) Tungler, A.; Fodor, K. *Catal. Today* **1997**, *37*, 191.
(4) Glorius, F.; Spielkamp, N.; Holle, S.; Goddard, R.; Lehmann, C. W. *Angew. Chem., Int. Ed.* **2004**, *43*, 2850.

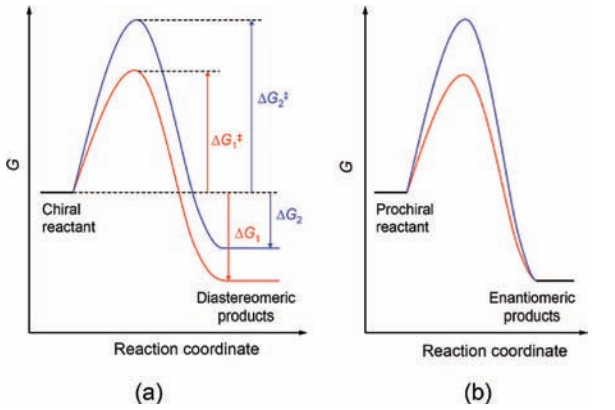

Figure 1. Energy profiles for diastereoselective (a) and enantioselective (b) reactions.

lytic hydrogenation of prochiral C═O bonds has received very little attention,[6] presumably because high diastereoselectivities are commonly obtained by hydrogenation with homogeneous chiral metal catalysts.

The origin of diastereoselectivity in hydrogenation is based on the chirality of the substrate itself. The chiral center can already be present on the backbone,[7] or a chiral auxiliary can be introduced.[8] Energetically different diastereomeric transition states ($\Delta G_1^{\ddagger} \neq \Delta G_2^{\ddagger}$) and products ($\Delta G_1 \neq \Delta G_2$) ensue from a chiral reactant even with an achiral catalyst, and the diastereomeric excess will be nonzero (Figure 1a). A chiral catalyst (or other chiral species) may enhance diastereoselectivity. Instead, a chiral catalyst is a prerequisite for energetically different diastereomeric transition states and asymmetric induction in transformations of a prochiral reactant (Figure 1b). In the absence of any chiral catalyst, the enantiomeric excess will be zero even under thermodynamic control due to the equal energies of the enantiomeric products.

Literature on heterogeneous catalytic hydrogenation is lacking detailed models, which would allow the prediction of stereoselectivity at the quantitative level as is the case of enantioselective homogeneous catalysis.[9] Qualitatively, a stereogenic center in the molecule influences the mode of adsorption of the molecule on the surface of the catalysts and, thus, the diastereofacial selectivity.[6b] Adsorption via the less hindered diastereotopic face of the molecule has been proposed. Therefore, the resulting diastereoselectivity depends crucially on the steric arrangement and conformational properties of the substrate molecule. The presence of a bulky substituent or polar group in the molecule, which directs the adsorption on the metal surface, is indispensable for obtaining high de's. Most of the substrates reported to date also have a certain backbone rigidity,[1] which limits their conformational degrees of freedom. For example, rigid ring structures, which can adsorb on the metal surface of a heterogeneous catalyst from only one of their diastereotopic faces, usually give higher de's.[6b] Hindered interconversion of the conformers of the substrate and intramolecular hydrogen bonds that stabilize some of the conformers may also affect the de. The de is also influenced by the catalytically active metal, the support, the solvent, and reaction conditions.

Scheme 1. Reaction Scheme of the Hydrogenation of 1-Phenyl-1,2-propanedione (PPD)[a]

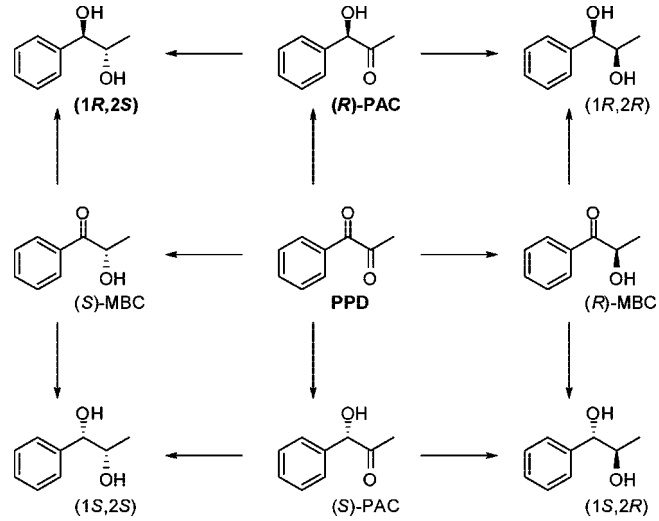

[a] Main products for hydrogenation over CD-modified Pt catalyst are indicated in bold.

Mechanistic studies are of fundamental importance in hydrogenation of chiral and prochiral molecules over heterogeneous catalysts. In ongoing work from our laboratories, kinetic and mechanistic aspects of the hydrogenation of prochiral diketones, in particular 1-phenyl-1,2-propanedione (PPD), over cinchona alkaloid-modified Pt catalysts have been investigated.[10] With cinchonidine as the chiral surface modifier, the main product obtained in PPD hydrogenation after the first step is (*R*)-1-hydroxy-1-phenyl-2-propanone [(*R*)-phenylacetylcarbinol or (*R*)-PAC][11] with maximum 70% enantiomeric excess (ee).[10c] Enantioselectivity depends prominently on the choice of reaction conditions (*c*, *p*, *T*), solvent, and modifier structure. Overall, hydrogenation of PPD produces a mixture of all possible enantiomeric hydroxyketones and diols, further complicating the mechanistic interpretation (Scheme 1). First, two regioisomeric α-hydroxyketones, 1-hydroxy-1-phenyl-2-propanone and 2-hydroxy-1-phenyl-1-propanone, are formed, both existing as their (*R*)- and (*S*)-enantiomers. Further hydrogenation of the hydroxyketones produces the corresponding (1*R*,2*R*)-, (1*S*,2*S*)-, (1*R*,2*S*)-, and (1*S*,2*R*)-1-phenyl-1,2-propanediols. In general, the

(5) Besson, M.; Blanc, B.; Champelet, M.; Gallezot, P.; Nasar, K.; Pinel, C. *J. Catal.* **1997**, *170*, 254.
(6) For reviews, see: (a) Besson, M.; Pinel, C. *Top. Catal.* **1998**, *5*, 25. (b) Kukula, P.; Prins, R. *Top. Catal.* **2003**, *25*, 29. (c) Besson, M.; Pinel, C. *Top. Catal.* **2003**, *25*, 43.
(7) (a) van der Waal, J. C.; van Bekkum, H.; Vital, J. M. *J. Mol. Catal. A: Chem.* **1996**, *105*, 185. (b) Huffman, M. A.; Reider, P. J. *Tetrahedron Lett.* **1999**, *40*, 831. (c) Guidotti, M.; Conti, L.; Fusi, A.; Ravasio, N.; Psaro, R. *J. Mol. Catal. A* **2002**, *182*−*183*, 151. (d) Jacob, R. G.; Perin, G.; Loi, L. N.; Pinno, C. S.; Lenardao, E. J. *Tetrahedron Lett.* **2003**, *44*, 3605. (e) Gini, F.; Del Moro, F.; Macchia, F.; Pineschi, M. *Tetrahedron Lett.* **2003**, *44*, 8559.
(8) Besson, M.; Gallezot, P.; Neto, S.; Pinel, C. *Tetrahedron: Asymmetry* **2000**, *11*, 1809.
(9) (a) Feldgus, S.; Landis, C. R. *J. Am. Chem. Soc.* **2000**, *122*, 12714. (b) Feldgus, S.; Landis, C. R. *Organometallics* **2001**, *20*, 2374.
(10) See, for example: (a) Toukoniitty, E.; Mäki-Arvela, P.; Kuzma, M.; Villela, A.; Kalantar Neyestanaki, A.; Salmi, T.; Sjöholm, R.; Leino, R.; Laine, E.; Murzin, D. Yu. *J. Catal.* **2001**, *204*, 281. (b) Toukoniitty, E.; Busygin, I.; Leino, R.; Murzin, D. Yu. *J. Catal.* **2004**, *227*, 210. (c) Busygin, I.; Toukoniitty, E.; Sillanpää, R.; Murzin, D. Yu.; Leino, R. *Eur. J. Org. Chem.* **2005**, 2811. (d) Busygin, I.; Nieminen, V.; Taskinen, A.; Sinkkonen, J.; Toukoniitty, E.; Sillanpää, R.; Murzin, D. Yu.; Leino, R. *J. Org. Chem.* **2008**, *73*, 6559.
(11) (R)-PAC is an important intermediate for the synthesis of ephedrines and pseudoephedrines, which are major ingredients in several pharmaceuticals used as anti-asthmatics, vasoconstricting agents and nasal decongestants. See: Subramanian, P. M.; Chatterjee, S. K.; Bhatia, M. C. *J. Chem. Technol. Biotechnol.* **1987**, *39*, 215.

enantioselectivities obtained in the hydrogenation of vicinal diketones over the cinchona alkaloid-modified Pt catalysts are inferior to those observed in the classical Orito reaction, that is, hydrogenation of methyl and ethyl pyruvates and other α-ketoesters.[12] Furthermore, the enantiodifferentiating mechanisms operating in the two systems (hydrogenation of ketoesters versus diketones) are different.[13]

To further elucidate the mechanism of PPD hydrogenation over chirally modified Pt catalysts and the origin of asymmetric induction in heterogeneous catalysis in general, the hydrogenation of enantiomerically enriched (*R*)-PAC (ee = 95%) over cinchonidine modified and unmodified Pt/Al_2O_3 was studied here. In earlier studies, Baiker et al.[14] investigated the hydrogenation of prochiral α-hydroxyketones over chirally modified heterogeneous catalyst systems, while Nieminen et al.[15] studied theoretical aspects of interactions between chiral α-hydroxyketones and cinchona alkaloids on Pt. In the present study, the issues of diastereoselectivity in the hydrogenation of chiral α-hydroxyketones over unmodified catalysts were investigated theoretically for the first time. The following questions were specifically addressed: (1) How does a chiral center in a substrate control its chemisorption on metal, (2) what is the detailed reaction mechanism of C=O hydrogenation, and (3) what is the origin of asymmetric induction? First, the kinetics of (*R*)-PAC hydrogenation over the Pt catalyst is presented. Second, adsorption of (*R*)-PAC on the Pt(111) surface and the whole reaction paths for (*R*)-PAC hydrogenation are examined computationally using density functional theory[16] (DFT). Third, DFT calculations on other chiral α-hydroxyketones, (*R*)-3-hydroxy-2-butanone and (*R*)-2-hydroxy-1-cyclohexanone, are performed to study the effect of the molecular structure of the substrate on the modes and energies of chemisorption for surface intermediates, along with overall reaction energies for each of the proposed elementary steps. Finally, qualitative estimations about the diastereoselectivities of the hydrogenation reactions are made on the basis of theoretically obtained stabilities of the stable reaction intermediates leading to the diastereomeric products.

2. Materials and Methods

2.1. Catalytic Hydrogenations. (*R*)-PAC for catalytic hydrogenations was obtained by pyruvate decarboxylases-catalyzed synthesis and purified by flash chromatography. The detailed preparation procedure is available in the Supporting Information. Purity of the obtained product was analyzed by chiral GC and HPLC (ee = 95%). NMR spectra are well in line with the literature.[10a] Catalytic experiments were carried out in a pressurized batch reactor (Parr, 300 cm^3). A commercial 5 wt % Pt/Al_2O_3 catalyst (Strem Chemicals, 78-1660) was used in hydrogenation. The detailed catalyst characterization and the pretreatment procedures are provided elsewhere.[10a] Toluene (J. T. Baker, 8077, >99.5%) and acetic acid (J. T. Baker, 6052, 99.9%) were used as solvents. The hydrogen pressure was 10 bar, and the temperature was 15 and 17 °C for the reaction in toluene and in acetic acid, respectively. The catalyst amount and liquid volume were 100 mg and 100 cm^3, and the stirring rate was 2000 rpm. In the experiments with the chiral modifier, the preactivated catalyst and solvent (50 cm^3) containing dissolved cinchonidine (3.4×10^{-5} mol, 10 mg) were loaded into the reactor and flushed with hydrogen for 10 min at 1 bar. The reactant solution (50 or 100 cm^3 in the case of unmodified catalyst) was saturated with hydrogen for 10 min in a separate injection chamber and injected into the reactor whereafter the reaction was started immediately. The initial concentrations of (*R*)-PAC and the modifier were 3.1×10^{-3} and 3.4×10^{-4} mol dm^{-3}, respectively. Samples were withdrawn from the reactor at different time intervals and analyzed with a Varian 3300 gas chromatograph (GC) equipped with a chiral column (β-Dex 225).

2.2. Theoretical Calculations. All DFT calculations were performed with the program package TURBOMOLE V5.9[17] using the BP86 gradient-corrected exchange-correlation functional[18] in combination with the Multipole-Accelerated-Resolution-of-Identity-*J* (MARI-*J*) approximation.[19] The BP86 functional has previously been used to study, for example, the mechanism of benzene hydrogenation on Pt(111).[20] Relativistic effects were taken into account implicitly using the relativistic effective core potential (ECP) from the TURBOMOLE library ("def-ecp") to represent the 60 core electrons of Pt.[21] The 18 valence electrons of platinum and all electrons of the other elements were treated explicitly using the SV(P) or the SVP basis set ("def-SV(P)" and "def-SVP").[22] The following convergence criteria were used: 10^{-6} hartree for the SCF energy; total energy up to 10^{-5} hartree; and maximum norm of Cartesian gradient up to 10^{-3} atomic units (bohr) for structure optimization.

Adsorption of α-hydroxyketones and their reaction with hydrogen on the Pt(111) surface were studied using the cluster model approach. Clusters consisting of two layers and 31 or 38 atoms were employed to model the Pt(111) surface. They were large enough to accommodate a reactant molecule and two hydrogen atoms but small enough that computations were feasible. To study the effect of cluster size on chemisorption, some calculations were also performed using clusters with two layers and 19 or 64 Pt atoms as well as three layers and 37 Pt atoms (Figure S1, Supporting Information). The two-layer clusters employed are denoted formally as $Pt_{12.7}$, $Pt_{19.12}$, $Pt_{23.15}$, and $Pt_{37.27}$, where *X* (*Y*) is the number of Pt atoms on the top (bottom) layer of the $Pt_{X.Y}$ cluster. The three-layer cluster is $Pt_{19.12.6}$. Hereafter, they are labeled in the text as Pt_N, where *N* indicates the total number of Pt atoms in the cluster.

To account for surface relaxation effects, the central atoms (i.e., atoms not on edges) on the top layer of the clusters were allowed to fully optimize. All other atoms were fixed at the crystal bulk structure with the Pt−Pt distance of 277.5 pm. To study the effect of surface relaxation on adsorption, totally fixed clusters were also used. Transition states for hydrogenation reactions and hydrogen diffusion on Pt were searched using constrained optimizations,

(12) For reviews, see: (a) Webb, G.; Wells, P. B. *Catal. Today* **1992**, *12*, 319. (b) Studer, M.; Blaser, H.-U.; Exner, C. *Adv. Synth. Catal.* **2003**, *345*, 45.
(13) (a) Murzin, D. Yu.; Mäki-Arvela, P.; Toukoniitty, E.; Salmi, T. *Cat. Rev.-Sci. Eng.* **2005**, *47*, 175. (b) Busygin, I.; Wärnå, J.; Toukoniitty, E.; Murzin, D. Yu.; Leino, R. *J. Catal.* **2008**, *254*, 339. (c) Busygin, I.; Tkachenko, O. P.; Nieminen, V.; Borovkov, V. Yu.; Sillanpää, R.; Toukoniitty, E.; Murzin, D. Yu; Kustov, L. M.; Leino, R. *J. Phys. Chem. C* **2007**, *111*, 9374.
(14) Sonderegger, O. J.; Ho, G. M.-W.; Bürgi, T.; Baiker, A. *J. Mol. Catal. A: Chem.* **2005**, *239*, 49.
(15) Nieminen, V.; Taskinen, A.; Toukoniitty, E.; Hotokka, M.; Murzin, D. Yu. *J. Catal.* **2006**, *237*, 131.
(16) Parr, R. G.; Yang, W. *Density-Functional Theory of Atoms and Molecules*; Oxford University Press: New York, 1989.
(17) (a) Ahlrichs, R.; Bär, M.; Häser, M.; Horn, H.; Kölmel, C. *Chem. Phys. Lett.* **1989**, *162*, 165. (b) Treutler, O.; Ahlrichs, R. *J. Chem. Phys.* **1995**, *102*, 346. (c) von Arnim, M.; Ahlrichs, R. *J. Comput. Chem.* **1998**, *19*, 1746.
(18) (a) Perdew, J. P. *Phys. Rev. B* **1986**, *33*, 8822. (b) Perdew, J. P. *Phys. Rev. B* **1986**, *34*, 7046. (c) Becke, A. D. *Phys. Rev. A* **1988**, *38*, 3098.
(19) (a) Eichkorn, K.; Treutler, O.; Öhm, H.; Häser, M.; Ahlrichs, R. *Chem. Phys. Lett.* **1994**, *240*, 283. (b) Eichkorn, K.; Treutler, O.; Öhm, H.; Häser, M.; Ahlrichs, R. *Chem. Phys. Lett.* **1995**, *242*, 652. (c) Eichkorn, K.; Weigend, F.; Treutler, O.; Ahlrichs, R. *Theor. Chem. Acc.* **1997**, *97*, 119. (d) Sierka, M.; Hogekamp, A.; Ahlrichs, R. *J. Chem. Phys.* **2003**, *118*, 9136.
(20) (a) Saeys, M.; Reyniers, M.-F.; Neurock, M.; Marin, G. B. *J. Phys. Chem. B* **2003**, *197*, 3844. (b) Saeys, M.; Reyniers, M.-F.; Neurock, M.; Marin, G. B. *J. Phys. Chem. B* **2005**, *109*, 2064.
(21) Andrae, D.; Häussermann, U.; Dolg, M.; Stoll, H.; Preuss, H. *Theor. Chim. Acta* **1990**, *77*, 123.
(22) Schäfer, A.; Horn, H.; Ahlrichs, R. *J. Chem. Phys.* **1992**, *97*, 2571.

where the interatomic distance representing the reaction coordinate was fixed while all other degrees of freedom were optimized. The transition state was characterized by the configuration with the highest energy along the reaction coordinate. This procedure for determining the transition state of relatively large adsorbates has been stated to yield energy barriers of reasonable accuracy, as compared to more rigorous methods, such as the nudged elastic band method.[23]

It has been stated that a low-spin state should be chosen to represent the electronic structure of a nonmagnetic metal surface (as Pt) and that it is customary to use the lowest energy low-spin cluster electronic state for the naked clusters as well as for the cluster together with its corresponding adsorbate.[24] In this study, all calculations were performed spin unrestricted with the spin state $S = 3$ (six extra up-spin orbitals) for the cluster per se and for the cluster with the adsorbate with even number of electrons. $S = 3$ represents the minimum energy spin state between $S = 0$ and 10 for the relaxed Pt_{31} cluster.[25] For systems with odd number of electrons, spin state $S = 5/2$ was used. These choices were respected even if in some cases the minimum energy spin state of the bare cluster or the cluster together with the adsorbate(s) had differed from $S = 3$.[26]

The adsorption energies were calculated using the equation

$$\Delta E_{ads} = E_{adsorbate+cluster} - E_{adsorbate} - E_{cluster} \quad (1)$$

where $E_{adsorbate+cluster}$ is the total electronic energy of the optimized adsorbate on the cluster, and $E_{adsorbate}$ and $E_{cluster}$ are the total electronic energies of the optimized, isolated adsorbate and naked cluster, respectively. Enthalpies or Gibbs energies of adsorption were not considered because calculation of the vibrational frequencies for the adsorbed molecules studied here was computationally too demanding.

Preliminary geometries of α-hydroxyketones on the Pt(111) surface were modeled by molecular mechanics[27] (MM) with the COMPASS (Condensed-phase Optimized Molecular Potentials for Atomistic Simulation Studies) force field[28] as implemented in the Forcite molecular mechanics module in Materials Studio 4.1 (Accelrys Software Inc.). As the force fields cannot properly model chemisorption and, consequently, exact structures of the adsorbed molecules, the role of the metal surface in the MM calculations was mainly to act as a steric constraint, similarly as in recent studies.[15,29] In this study, the flat Pt(111) surface was represented by a three-layer thick slab of dimensions 3.4 nm × 3.3 nm containing 182 platinum atoms in the upper- and lowermost layers and 195 atoms in the middle. During the calculations, all Pt−Pt distances were kept fixed to the experimental value of 277.5 pm of bulk Pt. The atomic charges of the adsorbates were determined using the QEq charge equilibration method[30] as implemented in Materials Studio (cf., also refs 15 and 29). The charges of all Pt atoms were set to zero.

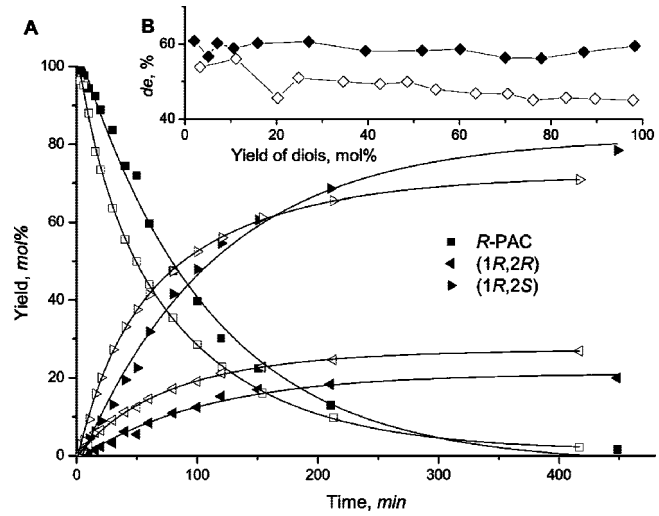

Figure 2. Kinetics profiles (A) and diastereoselectivity (B) in the hydrogenation of (*R*)-PAC over cinchonidine modified (filled symbols) and unmodified (empty symbols) Pt/Al_2O_3 in toluene.

Table 1. Heterogeneous Hydrogenation of PPD and (*R*)-PAC over Pt/Al_2O_3 Catalysts in Toluene

	initial rate[a]		diastereoselectivity	
modifier	PPD	(*R*)-PAC	de[b]	dr[c]
	212[d]	4.60	49	−[e]
cinchonidine	186[d]	1.65	60	58

[a] 10^{-5} mol min^{-1} g^{-1}_{cat}. [b] Diastereoselectivity in the hydrogenation of enantiomerically enriched (*R*)-PAC (ee = 95%); de (%) = 100 × ([1*R*,2*S*] − [1*R*,2*R*])/([1*R*,2*S*] + [1*R*,2*R*]). [c] Diastereoselectivity in the hydrogenation of (*R*)-PAC as estimated from the PPD hydrogenation experiments (see ref 13b); dr (%) = 100 × (k_{RS} − k_{RR})/(k_{RS} + k_{RR}), where k_{RS} and k_{RR} are apparent rate constants. [d] Reference 10b. [e] Not available.

3. Results and Discussion

3.1. Catalytic Hydrogenations. Hydrogenation of (*R*)-PAC produces two diastereomers, (1*R*,2*S*)-1-phenyl-1,2-propanediol and (1*R*,2*R*)-1-phenyl-1,2-propanediol, called (1*R*,2*S*)-diol and (1*R*,2*R*)-diol henceforward (Scheme 1). When (*R*)-PAC was hydrogenated over the unmodified platinum catalyst, significant diastereoselectivity was reached; the (1*R*,2*S*)-diol was formed in excess over the (1*R*,2*R*)-diastereomer with de of 49% (Figure 2). When cinchonidine was introduced into the reaction milieu, the diastereomeric excess increased to the value of 60%. This value is in very good agreement with the de of (*R*)-PAC hydrogenation estimated from the PPD hydrogenation experiments under similar reaction conditions using the kinetic approach (Table 1).[13b]

The initial rate of (*R*)-PAC hydrogenation over the cinchonidine-modified platinum catalyst in toluene was almost 3 times lower than the rate of (*R*)-PAC hydrogenation over the unmodified catalyst and 2 orders of magnitude lower than the rate of analogous hydrogenation of PPD (Table 1). Hydrogenation of (*R*)-PAC in acetic acid proceeded at an extremely low rate. After 18 h of reaction mixture treatment with hydrogen, no detectable amount of diols was found by GC analysis. These data are in agreement with hydrogenation of PPD in the same media.[10b]

3.2. Theoretical Investigation of Hydrogenation of (*R*)-PAC. (*R*)-PAC is a conformationally flexible molecule as indicated by the low energy barriers for the rotations τ_1 and τ_2 around its single bonds (Scheme 2).[15] Therefore, it is difficult to judge a priori which diastereotopic face, *re* or *si*, is more easily exposed

(23) Alcalá, R.; Greeley, J.; Mavrikakis, M.; Dumesic, J. A. *J. Chem. Phys.* **2002**, *116*, 8973.
(24) Illas, F.; Sousa, C.; Gomes, J. R. B.; Clotet, A.; Ricart, J. M. Elementary Steps of Catalytic Processes on Metallic and Bimetallic Surfaces. In *Theoretical Aspects of Heterogeneous Catalysis*; Nascimento, M. A. C., Ed.;Progress in Theoretical Chemistry and Physics; Kluwer Academic Publishers: Dordrecht, The Netherlands, 2001; Vol. 8, pp 149−181.
(25) Nieminen, V.; Taskinen, A.; Hotokka, M.; Murzin, D. Yu. *J. Catal.* **2007**, *245*, 228.
(26) More justification for using $S = 3$ with other Pt clusters can be found in refs 25 and 29.
(27) See, for example: Cramer, C. J. *Essentials of Computational Chemistry - Theories and Models*; Wiley: Chichester, U.K., 2002; p 17.
(28) Sun, H. *J. Phys. Chem. B* **1998**, *102*, 7338.
(29) Taskinen, A.; Nieminen, V.; Hotokka, M.; Murzin, D. Yu. *J. Phys. Chem. C* **2007**, *111*, 5128.
(30) Rappé, A. K.; Goddard, W. A., III. *J. Phys. Chem.* **1991**, *95*, 3358.

Scheme 2. Numbering of Atoms Used for Defining Torsion Angles in (*R*)-PAC, Illustration of the Three Nonequivalent Carbon Atoms of the Phenyl Moiety as a Result of Adsorption at the Bridge(30) Site of the Pt(111) Surface, and the η^2 Adsorption Mode of the C═O Moiety with Different Positions for Attacking Hydrogen Atoms (H_a, H_b, H_c, H_d)

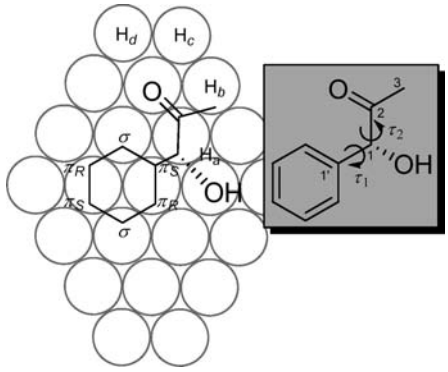

to the metal surface and, especially, any quantitative value for the de. Basically, stereoselection originates from thermodynamic and kinetic factors such as the relative thermodynamic stabilities of the diastereomeric adsorption modes and the difference in the reaction rate of those species. The inherently unequal thermodynamic stabilities of the product diastereomers may also contribute to the stereoselection. In the following sections, results concerning these issues are presented.

3.2.1. Thermodynamic Stabilities of the Products. In the most stable gas-phase conformer of (*R*)-PAC, the whole O═C−C−OH system adopted a planar *s-cis*-like conformation due to the stabilization by an intramolecular hydrogen bond.[15] This structure was used as the starting point for searching the most stable conformations of (1*R*,2*R*)- and (1*R*,2*S*)-diols in the gas phase. Geometries of totally eight conformers (four per one diastereomer) varying with respect to the torsion angle O−C−C−O (ca. +50 or −50°) and having an intramolecular hydrogen bond (OH···OH) were optimized at the BP86/SV(P) level of theory using the MARI-J approximation (Figure S2). Vibrational frequencies for the two most stable structures, (a) and (e) in Figure S2, were calculated to ensure that the geometries represented true minima on the potential energy surface. The calculations predicted that (1*R*,2*R*)-diol is more stable than (1*R*,2*S*)-diol by 3 kJ mol^{-1}. This result would imply an excess formation of (1*R*,2*R*)-diol, assuming that the reaction is under simple thermodynamic control (i.e., product composition is governed by the equilibrium thermodynamics) and that the difference between the total electronic energies of the diastereomers corresponds to the difference between their Gibbs energies. However, the predominant formation of (1*R*,2*S*)-diol was observed in the experiments. Therefore, a detailed investigation of the influence of the catalytic Pt surface on product distribution is presented below.

3.2.2. Adsorption of (*R*)-PAC. A tentative, qualitative analysis of (*R*)-PAC adsorption on Pt surface yielded four essentially different adsorption modes (see Supporting Information and Figure S3). The most stable, DFT optimized geometries of these main modes are shown in Figure 3.

To fully characterize the adsorption of such a complex molecule as (*R*)-PAC, a few issues have to be introduced. First, (*R*)-PAC may be considered as a combination of functional groups (aromatic, alcohol, ketone), each of which has its own characteristic adsorption behavior. Especially, each functional group may be adsorbed at several surface sites. For example, at low surface coverage the most stable adsorption site of benzene on Pt(111) is the so-called bridge(30) with an adsorption energy of ca. −120 kJ mol^{-1} (Scheme 2), whereas the next most stable hollow(0) sites are less stable by a few dozens of kJ mol^{-1}.[25,31,32] The most stable adsorption modes of (*R*)-PAC are expected to have a bridge(30) adsorbed phenyl ring just as in the case of PPD adsorption.[25] Therefore, such modes are focused on in the current study.

The second issue of (*R*)-PAC adsorption is attributed to the fact that the distortion of benzene upon adsorption at the bridge(30) site yields three nonequivalent carbon atoms (Scheme 2). The aromatic C atoms involved in π-type interactions with Pt will be referred to as π-type within this Article, whereas the other C atoms will be refferred to as σ-type.[31] Moreover, the adjacent π-type carbons are distinguished by their chirality and are assigned to π_R- and π_S-type according to the Cahn−Ingold−Prelog convention.[33,34] The aromatic carbon atom bonded to the aliphatic moiety of (*R*)-PAC (i.e., *ipso*-carbon) can be any one of these three types (σ, π_R, and π_S), most likely yielding three different adsorption energies. Therefore, the effect of *ipso*-carbon type was investigated for all four main adsorption modes of (*R*)-PAC.

The third issue of (*R*)-PAC adsorption is related to the detailed structure of the Pt(111) surface. Each adsorption mode may be oriented in two ways on the Pt(111) surface, which complicates the study of adsorption further. The distinction between the two orientations can be described by first recognizing that the Pt−Pt "bridge" divides the bridge(30) adsorbed Ph ring into two almost equal halves, of which one can be seen as residing over an hcp-hollow site, whereas the other lies over an fcc-hollow site (Figure S4). The *ipso*-carbon, while retaining its chirality, can be situated in either of the halves depending on the adsorption orientation. In this Article, more stable adsorption orientations are discussed and the reaction energy profiles for *re*- and *si*-face hydrogenation [yielding (1*R*,2*R*)- and (1*R*,2*S*)-diols, respectively, cf., below] have been calculated using the adsorption modes with more stable orientation (i.e., with *ipso*-carbon over an hcp-hollow site). Further details of the effect of adsorption mode orientation can be found in the Supporting Information.

The fourth issue of adsorption is related to the cluster used to model the Pt(111) surface. Not only the size and shape of the cluster (number of atomic layers and number of atoms in each layer) used to model the metal surface may have an effect on the adsorption energy but also whether the adsorbate is adsorbed on the edge or the center of the cluster (edge effects). A detailed summary of the effects of cluster size on the adsorption of (*R*)-PAC, its hydrogenation intermediates, and products on Pt(111) is given in the Supporting Information. Here, it is just noted that our choices of clusters are justified and do not affect the conclusions about diastereoselectivity of the hydrogenation reaction, one of the main objects in the present work.

Twenty different adsorption modes with the bridge(30) site adsorption of the phenyl ring leading to both (1*R*,2*R*)- and (1*R*,2*S*)-diols were considered by DFT at the BP86/SV(P) level using the MARI-*J* approximation (Tables 2 and S2, Figures 3 and S5). The adsorption modes are labeled according to the

(31) Saeys, M.; Reyniers, M.-F.; Marin, G. B.; Neurock, M. *J. Phys. Chem. B* **2002**, *106*, 7489.
(32) Morin, C.; Simon, D.; Sautet, P. *J. Phys. Chem. B* **2004**, *108*, 12084.
(33) Cahn, R. S.; Ingold, C.; Prelog, V. *Angew. Chem., Int. Ed. Engl.* **1966**, *5*, 385.
(34) Prelog, V.; Helmchen, G. *Angew. Chem., Int. Ed. Engl.* **1982**, *21*, 567.

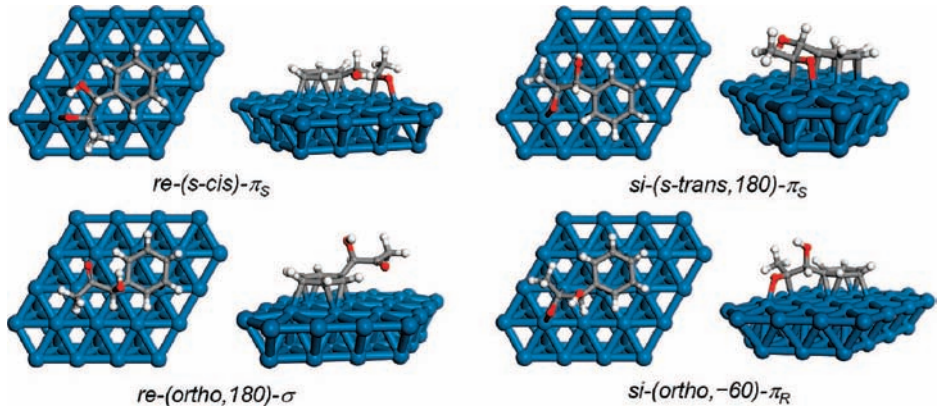

Figure 3. Top and side views of the four main adsorption modes of (*R*)-PAC on the Pt_{38} cluster. The structures were optimized at the BP86/SV(P) level of theory.

Table 2. Adsorption Energy (ΔE_{ads}), Sum of π and π^* Orbital Energies (ΔE_{orb} for α Spin; for β Spin Essentially the Same Energies) Relative to That for the *si*-(*s-trans,180*)-π_S Mode, and C═O Bond Distances and Torsion Angles for Different Adsorption Modes of (*R*)-PAC with a Bridge(30) Adsorbed Phenyl Moiety on the (111) Surface of a Relaxed Pt_{38} Cluster Calculated at the BP86/SV(P) Level of Theory[a]

adsorption mode	ΔE_{ads} (kJ mol^{-1})	ΔE_{orb} (kJ mol^{-1})	C═O (pm)	φ (deg)[b]
re-(*s-cis*)-π_S	−135 (−76)[c]	22 (23)	136 (135)	125 (125)
re-(*s-cis*)-π_R	−128		137	121
re-(*s-cis*)-σ	−117		123	177
re-(*s-cis*)-π_S-η^0(*CO*)	−107	89	124	159
si-(*s-trans,180*)-π_S	−129 (−65)	0 (0)	134 (133)	−131 (−133)
si-(*s-trans,0*)-π_S	−89		135	−129
si-(*s-trans,−60*)-π_S	−102		135	−128
si-(*s-trans,180*)-π_R	−115		123	−174
si-(*s-trans,180*)-σ	−129	172	122	−175
si-(*s-trans,180*)-π_S-η^0(*CO*)	−110	132	123	−167
re-(*ortho,180*)-π_S	−92	114	123	170
re-(*ortho,180*)-π_R	−91	34	135	131
re-(*ortho,60*)-π_R	−81	41	134	135
re-(*ortho,180*)-σ	−99	138	123	172
re-(*ortho,60*)-σ	−85	160	122	175
si-(*ortho,−60*)-π_S	−72		123	−171
si-(*ortho,−60*)-π_R	−104	22	136	−128
si-(*ortho,60*)-π_R	−96	24	136	−129
si-(*ortho,−60*)-σ	−80	107	123	−178
si-(*ortho,60*)-σ	−74	141	123	−180

[a] More details of the adsorption modes (e.g., the adsorption site of *ipso*-carbon) can be found in Table S2. [b] φ = ∠(C1,C2,C3,O2), indicates distortion from planarity: $|\varphi| = 180° \Rightarrow$ planar; $|\varphi| = 120° \Rightarrow$ tetrahedral (see Scheme 2). [c] The values on a rigid Pt_{38} cluster are given in parentheses.

diastereotopic face of the carbonyl group exposed to the platinum surface (*re* or *si*), the position of the hydroxyl group relative to the carbonyl group (*s-cis*, *s-trans*, *ortho*), an approximate value for the torsion angle H−C−O−H in the optimized structure (0, ±60, ±120, 180), and the type of *ipso*-carbon (σ, π_R, π_S). In the two thermodynamically most stable adsorption modes, the C−OH bond was nearly parallel to the platinum surface, synperiplanar relative to the carbonyl group adsorbed by its *re*-face [*re*-(*s-cis*)-π_S, $\Delta E_{ads} = -135$ kJ mol^{-1}] and antiperiplanar relative to the carbonyl group adsorbed by its *si*-face [*si*-(*s-trans,180*)-π_S, $\Delta E_{ads} = -129$ kJ mol^{-1}]. The most stable *re*-(*s-cis*) mode had an internal hydrogen bond between the carbonyl and hydroxyl groups. Interaction between the hydroxyl group hydrogen of the *si*-(*s-trans*) mode and the Pt surface was stabilizing.

The most stable adsorption geometries of the modes where the hydroxyl group was roughly orthogonal to the CO moiety and the platinum surface were *re*-(*ortho,180*)-σ and *si*-(*ortho,−60*)-π_R. Their interaction with Pt was weaker than that for the most stable *re*-(*s-cis*) and *si*-(*s-trans*) adsorption modes by ca. 30 kJ mol^{-1}. This decrease in adsorption strength may be assigned, at least partly, to a lack of stabilizing interaction between the hydroxyl group and the metal surface. Within the *re*-(*ortho*) and *si*-(*ortho*) modes, the most stable adsorption geometries were those with the O−H bond pointing toward the carbonyl oxygen.

The effect of the type of the *ipso*-carbon on the adsorption energy was pronounced (Tables 2 and S2). For instance, within the *re*-(*s-cis*) adsorption mode, adsorption strength diminished in the following series of *ipso*-carbons: $\pi_S > \pi_R > \sigma$. The C═O bonds in *re*-(*s-cis*)-π_R and *re*-(*s-cis*)-π_S interacted strongly with the Pt surface, adopting the η^2 (di-σ) chemisorption mode (see the geometrical parameters in Table 2). Instead, interaction of the carbonyl moiety in *re*-(*s-cis*)-σ with the surface was weaker, which could explain the lower thermodynamic stability of that mode. Stabilization of the *re*-(*s-cis*)-π_S adsorption mode by chemisorption of the carbonyl moiety was pronounced; the change of the adsorption mode of C═O from η^2 to η^0 (not chemisorbed) was entailed by a decrease of 28 kJ mol^{-1} in the adsorption energy. More details on the effect of hydrogen bonding, *ipso*-carbon type, and phenyl ring adsorption site on (*R*)-PAC adsorption can be found in the Supporting Information.

Hydrogenation of the C═O double bond may be viewed as involving interactions between frontier molecular orbitals of the reacting species, that is, hydrogen 1s and carbonyl π orbitals as exemplified by the Bürgi−Dunitz trajectory for nucleophiles attacking the carbonyl moiety.[35] Vargas et al.[36] found that the hydrogenation rate of substituted acetophenones over Pt catalysts correlates with the stability of the reactive keto carbonyl π orbitals of the isolated substrates. The sum of bonding π and antibonding π^* orbital stabilization was proposed to be the most general parameter for measuring the reactivity.[36] The orbital stabilization results in lowering of the transition state energy, hence decreasing the activation energy and increasing the rate of the hydrogenation reaction. To evaluate the reactivity of various adsorption modes toward hydrogenation, the analysis

(35) (a) Bürgi, H. B.; Dunitz, J. D.; Shefter, E. *J. Am. Chem. Soc.* **1973**, *95*, 5065. (b) Bürgi, H. B.; Dunitz, J. D.; Lehn, J. M.; Wipff, G. *Tetrahedron* **1974**, *30*, 1563. (c) Liotta, C. L.; Burgess, E. M.; Eberhardt, W. H. *J. Am. Chem. Soc.* **1984**, *106*, 4849.
(36) (a) Vargas, A.; Bürgi, T.; von Arx, M.; Hess, R.; Baiker, A. *J. Catal.* **2002**, *209*, 489. (b) Vargas, A.; Bürgi, T.; Baiker, A. *New J. Chem.* **2002**, *26*, 807.

of the carbonyl π and π^* orbitals was performed using the Kohn−Sham (KS) orbitals (Figure S6).[37,38]

The results of the orbital analysis (Tables 2 and S2) suggested that hydrogenation of the *si*-(*s-trans*,*180*)-π_S adsorption mode is favored over the *re*-(*s-cis*)-π_S mode by virtue of its higher π and π^* orbital stabilization. Therefore, on the basis of the thermodynamic stabilities of the adsorption modes, the Pt catalyst surface will be more occupied by *re*- than *si*-face adsorbed species, but the *si*-face adsorbed species may undergo faster hydrogenation due to the lower energies of the carbonyl orbitals. To fully understand the origin of diastereoselectivity and product distribution in hydrogenation of (*R*)-PAC, it was necessary to study all elementary steps of the reaction.

3.2.3. Addition of Hydrogen. The mechanism of hydrogenation of the C═O double bond on the Pt surface has been investigated before experimentally and by DFT.[23,39a,40−48] The reaction path has been thought to involve a series of surface-catalyzed hydrogen addition steps (i.e., stepwise addition) and is known as the Horiuti−Polanyi mechanism.[49] Two hydrogenation pathways have been considered in the literature: in one of them, a hydroxyalkyl species is formed by adding the first hydrogen atom to the oxygen atom of the C═O double bond, whereas in the other pathway, the carbonyl carbon atom is attacked by the first hydrogen atom, forming an alkoxy species (Scheme 3). The second hydrogenation step leads to the product alcohol in both cases. In addition to these pathways, a pairwise addition mechanism, where both hydrogen atoms attack the C═O bond simultaneously (Scheme 3), was studied in this work.

To make computations of reaction energetics feasible, the Pt_{31} cluster was chosen to represent the catalyst surface. The two most stable adsorption modes of (*R*)-PAC, that is, *re*-(*s-cis*)-π_S and *si*-(*s-trans*,*180*)-π_S, were selected to undergo hydrogenation. They give diastereomeric (1*R*,2*R*)- and (1*R*,2*S*)-diols upon addition of two hydrogen atoms, respectively. In the potential energy profiles for the feasible pathways for the hydrogenation (Figures 4 and 5), the starting point (**A**, $E = 0$ kJ mol^{-1}) refers to gas-phase (*R*)-PAC, gas-phase hydrogen (H_2), and the bare Pt_{31} cluster. The first two steps of hydrogenation consisted of the dissociative adsorption of hydrogen at atop sites (**A** → **B**) and molecular adsorption of (*R*)-PAC (**B** → **C**). Adsorbed (*R*)-PAC and two hydrogen atoms at an infinite separation from each other (**C**) represent a reference adsorption state for the system where the intermolecular interactions between the adsorbed species (lateral interactions) are negligible. The adsorption and desorption steps were assumed to be nonactivated. After a hydrogen molecule was dissociatively adsorbed far away from (*R*)-PAC, a dissociated hydrogen atom was assumed to approach the carbonyl group. The binding energies of the hydrogen atom are about the same for various adsorption sites on Pt(111), and due to the very low diffusion barriers, the hydrogen can move quite freely on the surface at low coverage.[50]

Scheme 3. Possible Reaction Paths for the Hydrogenation of the C═O Double Bond on Pt(111)

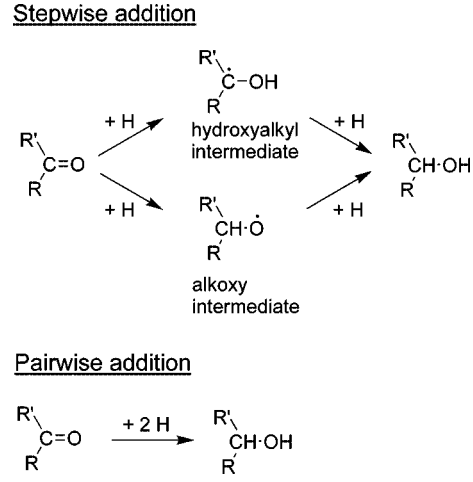

The main points of the hydrogenation pathways studied are reported here. More detailed information about various trajectories for hydrogen attack, interatomic distances, etc., can be found in the Supporting Information.

a. Hydroxyalkyl Hydrogenation Route. The minimum energy pathway from the reference state (**C**) via the hydroxyalkyl intermediate to the gas-phase product diol (**N**) was the following (Figures 4 and S8). For simplicity, hydrogen attack to the *si*-face leading to the (1*R*,2*S*)-diol will be discussed here in detail. Results for the *re*-face attack can be found in Figures 4 and S7 and Table S3.

First, the adsorbed (*R*)-PAC converted from the totally chemisorbed state (**C**) to the η^0(CO) state (**E**) with a hydrogen coadsorbate being a spectator at infinite distance. This change was associated with a low activation barrier of 11 kJ mol^{-1} (**D**). Second, adsorbed (*R*)-PAC-η^0(CO) (**E**) was in turn a spectator while hydrogen diffused from infinity from the direction of the H_c position (Scheme 2) to the atop position (**H**) by crossing over a barrier of 23 kJ mol^{-1} (**G**). The elementary step of hydrogen attack from the precursor state of the reaction (**H**) to the carbonyl oxygen (**J**) had a small activation energy of 23 kJ mol^{-1} (**I**, Figure S12) with a reaction energy $\Delta E_r = -30$ kJ mol^{-1}. Interestingly, the precursor state **H** was more stable than the reference state **C** by 11 kJ mol^{-1}. A similar type of a precursor state was reported when studying theoretically the hydrogenation pathways of acrolein on Pt(111).[47] Hence, the hydrogen attack took place at the C═O moiety not directly bonded to the surface, thus supporting an intermediate pathway between Langmuir−Hinshelwood and Eley−Rideal general types of mechanisms as proposed earlier.[47]

(37) Huang, P.; Carter, E. A. *Annu. Rev. Phys. Chem.* **2008**, *59*, 261.
(38) (a) Baerends, E. J.; Gritsenko, O. V. *J. Phys. Chem. A* **1997**, *101*, 5383. (b) Stowasser, R.; Hoffmann, R. *J. Am. Chem. Soc.* **1999**, *121*, 3414. (c) Kar, T.; Ángyán, J.; Sannigrahi, A. B. *J. Phys. Chem. A* **2000**, *104*, 9953. (d) Hamel, S.; Duffy, P.; Casida, M. E.; Salahub, D. R. *J. Electron Spectrosc. Relat. Phenom.* **2002**, *123*, 345.
(39) (a) Sen, B.; Vannice, M. A. *J. Catal.* **1988**, *113*, 52. (b) Vargas, A.; Bürgi, T.; Baiker, A. *J. Catal.* **2004**, *222*, 439. (c) Diezi, S.; Ferri, D.; Vargas, A.; Mallat, T.; Baiker, A. *J. Am. Chem. Soc.* **2006**, *128*, 4048. (d) Vargas, A.; Reimann, S.; Diezi, S.; Mallat, T.; Baiker, A. *J. Mol. Catal. A: Chem.* **2008**, *282*, 1.
(40) van Druten, G. M. R.; Ponec, V. *Appl. Catal., A: Gen.* **2000**, *191*, 153.
(41) van Druten, G. M. R.; Ponec, V. *Appl. Catal., A: Gen.* **2000**, *191*, 163.
(42) Greeley, J.; Mavrikakis, M. *J. Am. Chem. Soc.* **2002**, *124*, 7193.
(43) Greeley, J.; Mavrikakis, M. *J. Am. Chem. Soc.* **2004**, *126*, 3910.
(44) Desai, S. K.; Neurock, M.; Kourtakis, K. *J. Phys. Chem. B* **2002**, *106*, 2559.
(45) Hirschl, R.; Eichler, A.; Hafner, J. *J. Catal.* **2004**, *226*, 273.
(46) Loffreda, D.; Delbecq, F.; Vigné, F.; Sautet, P. *Angew. Chem., Int. Ed.* **2005**, *44*, 5279.
(47) Loffreda, D.; Delbecq, F.; Vigné, F.; Sautet, P. *J. Am. Chem. Soc.* **2006**, *128*, 1316.
(48) Rauls, E.; Hammer, B. *Catal. Lett.* **2006**, *106*, 111.
(49) Horiuti, J.; Polanyi, M. *Trans. Faraday Soc.* **1934**, *30*, 1164.
(50) Papoian, G.; Nørskov, J. K.; Hoffmann, K. *J. Am. Chem. Soc.* **2000**, *122*, 4129.

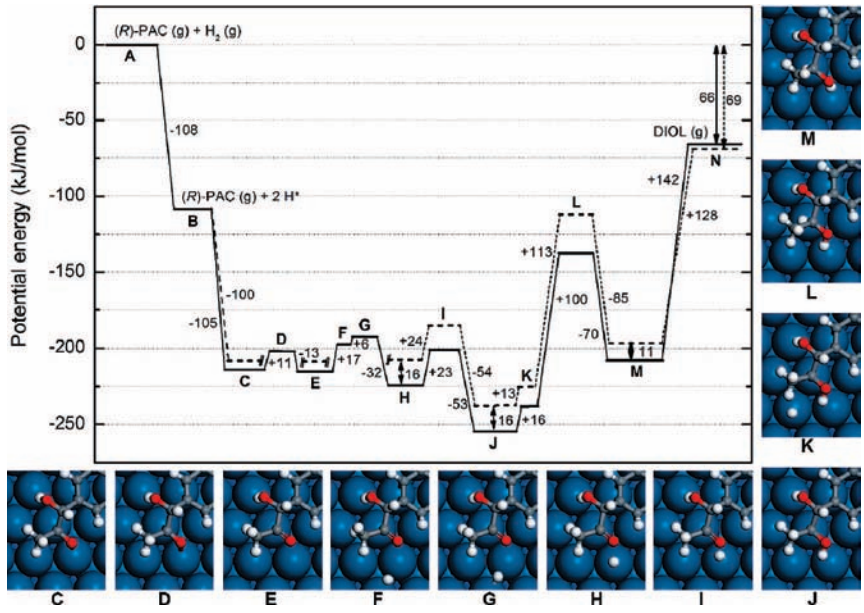

Figure 4. DFT (BP86/SVP) computed potential energy profile for the hydrogenation of (*R*)-PAC on Pt(111) involving the hydroxyalkyl intermediate (**J**). Represented are both *re*-face addition (dashed line) and *si*-face addition (solid line) leading to (1*R*,2*R*)- and (1*R*,2*S*)-diols, respectively. The reference state (**A**) is gas-phase (*R*)-PAC, H_2, and bare Pt_{31} cluster. Top views of the reaction intermediates and transition states are shown for the *si*-face addition. **C** and **E** are different adsorption modes of (*R*)-PAC; **F** and **H** are coadsorption states between (*R*)-PAC and hydrogen; **K** is a coadsorption state between monohydrogenated (*R*)-PAC (hydroxyalkyl intermediate) and hydrogen; **M** is adsorbed product diol. **D** and **G** represent transition states for the change of molecule's adsorption mode and hydrogen diffusion, respectively, while **I** and **L** represent the transition states for hydrogenation. Side views of the species **C**–**M** for *re*- and *si*-face addition are shown in Figures S7 and S8, respectively.

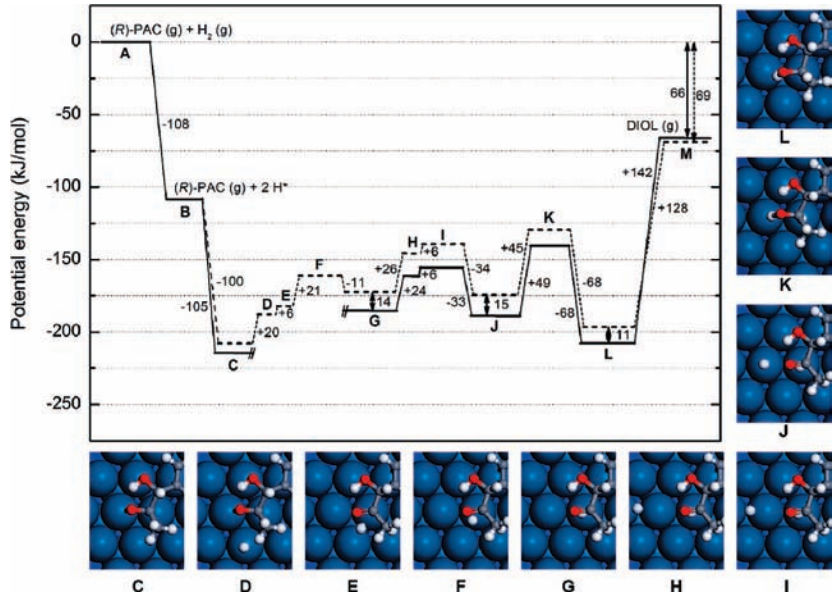

Figure 5. DFT (BP86/SVP) computed potential energy profile for the hydrogenation of (*R*)-PAC on Pt(111) through pairwise hydrogen addition. Represented are both *re*-face addition (dashed line) and *si*-face addition (solid line) leading to (1*R*,2*R*)- and (1*R*,2*S*)-diols, respectively. The reference state (**A**) is gas-phase (*R*)-PAC, H_2, and bare Pt_{31} cluster. Top views of the reaction intermediates and transition states are shown for the *re*-face addition. **C** is adsorbed (*R*)-PAC; **D**, **E**, and **G** are coadsorption states between (*R*)-PAC and hydrogen; **H** and **J** are coadsorption states between (*R*)-PAC and two hydrogen atoms; **L** is adsorbed product diol. **F** and **I** represent transition states for hydrogen diffusion, while **K** represents the transition state for hydrogenation. Side views of the species **C**−**L** for *re*- and *si*-face addition are shown in Figures S10 and S11, respectively.

After the hydroxyalkyl intermediate (**J**) was formed, the reaction continued by pulling the second hydrogen atom to the vicinity of the monohydrogenated product (**K**, position H_b in Scheme 2). The total activation barrier (**L**) including the hydrogen diffusion was rather high (E_a = 116 kJ mol^{-1}). The elementary step of hydrogen attack from infinity to the carbonyl carbon of the hydroxyalkyl intermediate (**J** → **M**) was endothermic by 46 kJ mol^{-1}. Desorption of the adsorbed product diol (**M**) to the gas-phase diol (**N**) was endothermic by 142 kJ mol^{-1}, and the whole reaction from the gas-phase reactants to the gas-phase product (1*R*,2*S*)-diol (**A** → **N**) was exothermic by 66 kJ mol^{-1}.

The hydroxyalkyl hydrogenation route has previously been studied theoretically by DFT for formaldehyde,[43−45] *trans*-acrolein,[47] and methyl pyruvate[48] on Pt(111). The reaction step from the adsorbed reactants to the adsorbed hydroxyalkyl intermediate was found to be exothermic by 25−44 kJ mol^{-1} having an activation energy barrier of 28−43 kJ mol^{-1} (with

one exceptionally high value of 83 kJ mol^{-1} by Desai et al.[44]), whereas the step from the hydroxyalkyl intermediate to the adsorbed product was determined to be endothermic by 15−26 kJ mol^{-1} with an activation energy of 79−108 kJ mol^{-1}.[43−45,47,48] The corresponding values for (*R*)-PAC hydrogenation, ΔE_r = −30 to −41 kJ mol^{-1} and E_a = 12−24 kJ mol^{-1} for the first step, and ΔE_r = 41−46 kJ mol^{-1} and E_a = 116−126 kJ mol^{-1} for the second step, were of magnitude similar to that of the previously reported values. The distances of the O−H and C−H bonds being formed in the transition states of (*R*)-PAC hydrogenation were 145−155 and 160−165 pm, respectively, being in agreement with *d*(O−H) = 160−194 pm (260 pm in ref 45) and *d*(C−H) = 146−184 pm in the transition states of acrolein and formaldehyde hydrogenation.[43−45,47]

The potential energy profiles for the *re*- and *si*-face hydrogenations of (*R*)-PAC were quite similar (Figure 4). However, some differences that could explain diastereoselection were observed. It is reasonable to assume that the energy barriers between **C** and **H** were of similar magnitude for both *re*- and *si*-face additions, inasmuch as the C═O desorption and hydrogen diffusion steps do not contribute to diastereodifferentiation. The adsorption of (*R*)-PAC through its *re*- and *si*-faces on a clean Pt(111) surface was thermodynamically almost equally favorable (Figure 4, Table S3). Although the difference of 5 kJ mol^{-1} between the adsorption energies of *re*-(*s-cis*)-π_S and *si*-(*s-trans*,*180*)-π_S would alone induce considerable diastereoselectivity (other parameters that could influence de being equal), it is rather small and could be within the limits of computational accuracy. However, the difference between the stabilities of the adsorption modes with a coadsorbed hydrogen atom (**H**) increased to 16 kJ mol^{-1} in favor of *si*-face adsorption. For comparison, this difference was 6 kJ mol^{-1} on Pt_{38}, also favoring *si*-face adsorption. Consequently, the preference for the *si*-face adsorption cannot be accounted for cluster size effects. Therefore, in a real catalytic system with a pool of surface atoms available for reaction, the surface is expected to be covered mainly by the *si*-(*s-trans*,*180*)-π_S mode.

The reaction step from the precursor state (**H**) to the hydroxyalkyl intermediate (**J**) was exothermic by 30 kJ mol^{-1} and had an activation energy of 23−24 kJ mol^{-1} for both *re*- and *si*-face addition. The monohydrogenated products were then formed at equal rates from the corresponding precursor states. In contrast, the energy barrier for addition of second hydrogen (**J** → **M**) was higher for *re*- than *si*-face addition by ca. 10 kJ mol^{-1}, thus implying a slower *re*-face addition. The overall reaction step **J** → **M** was less endothermic by 5 kJ mol^{-1} for the *re*-face addition (Table S3). The adsorbed (1*R*,2*R*)-diol was thermodynamically less stable than (1*R*,2*S*)-diol by 11 kJ mol^{-1}, and the desorption energy was 14 kJ mol^{-1} less for (1*R*,2*R*)-diol.

In conclusion, the formation of (1*R*,2*S*)-diol by the hydroxyalkyl hydrogenation route was strongly favored by thermodynamics (more stable adsorption) and kinetics (faster hydrogenation of the hydroxyalkyl intermediate). The desorption step had an effect on the gas-phase product selectivity in favor of (1*R*,2*R*)-diol. A key role in the C═O/C═C hydrogenation selectivity of acrolein was attributed to the desorption step of the products propanal and propenol.[47] However, the difference between their desorption energies (82 kJ mol^{-1}) was very large as compared to that of (1*R*,2*R*)- and (1*R*,2*S*)-diols (14 kJ mol^{-1}). Therefore, it is probable that the desorption step is not crucial in controlling the diastereoselectivity of (*R*)-PAC hydrogenation. In fact, this is supported by the experimental observation that the de does not depend on (*R*)-PAC conversion (Figure 2). Altogether, the theoretical results of the reaction energetics for hydrogenation of (*R*)-PAC via the hydroxyalkyl intermediate are qualitatively well in line with experimentally observed diastereoselectivity.

b. Alkoxy Hydrogenation Route. For simplicity, the attack of a hydrogen atom to the *re*-face of (*R*)-PAC is considered here in detail. Results for the *si*-face attack can be found in Figures 5 and S11 and Table S4. Starting from the reference state (**C**, Figures 5 and S10), the diffusion of one adsorbed hydrogen atom from its infinite position close to (*R*)-PAC gave a coadsorption state (**D**) with the hydrogen atom situated at an atop site (position H_b in Scheme 2). Thereafter, as in the case of hydroxyalkyl hydrogenation pathway, the C═O moiety decoordinated from the surface before interaction with the hydrogen atom, giving the coadsorption state (**E**). The following transfer of the hydrogen atom to the coadsorption state (**G**), where the atop hydrogen was coordinated to both carbonyl oxygen and carbon, was associated with an activation barrier (**F**) of 21 kJ mol^{-1}.

The next elementary step included the formation of the alkoxy intermediate from **G** with an activation barrier of 68 kJ mol^{-1} and reaction energy of 67 kJ mol^{-1} (not shown in Figure 5). The reaction could theoretically proceed further by addition of the second hydrogen at the carbonyl O atom. However, the alkoxy intermediates (Figure S9) had a very low barrier (1−6 kJ mol^{-1}) for the reverse dehydrogenation step, and the reaction energy for the step from the adsorbed reactants to the alkoxy intermediate was of the same magnitude with the desorption energy of (*R*)-PAC. Therefore, formation of the alkoxy intermediate is unlikely.

The alkoxy hydrogenation route has previously been studied theoretically with DFT for formaldehyde,[43−45] propanal and acetone,[23] *trans*-acrolein,[47] and methyl pyruvate[48] on Pt(111). The reaction step from the adsorbed reactants to the adsorbed alkoxy intermediate was found to be endothermic by 30−58 kJ mol^{-1} having an activation energy barrier between 38 and 61 kJ mol^{-1}, whereas the step from the alkoxy intermediate to the adsorbed product was determined to be exothermic by 53−65 kJ mol^{-1} with an activation energy of 14−30 kJ mol^{-1} (with one exceptionally high value of 77 kJ mol^{-1} by Desai et al.[44]). The corresponding values for (*R*)-PAC hydrogenation, ΔE_r = 85−103 kJ mol^{-1} and E_a = 91−104 kJ mol^{-1} for the first step, and ΔE_r = −(80−92) kJ mol^{-1} for the second step (transition state was not found, cf., below), were clearly larger than the previously reported values. The distance of the C−H bond formed in the first transition state of (*R*)-PAC hydrogenation was 127−129 pm, whereas in the transition states of acrolein, acetone, propanal, and formaldehyde hydrogenation, the bond distance was notably larger, *d*(C−H) = 140−168 pm[23,43,44,47] (239 pm for formaldehyde by Hirschl et al.[45]).

c. Pairwise Hydrogenation Route. The pairwise hydrogenation route was found while studying the addition of the second hydrogen atom to the alkoxy intermediate. No single transition state connecting the adsorbed alkoxy intermediate and the product diol was found; the previously formed C−H bond broke when the second hydrogen atom approached the carbonyl oxygen. Instead, a novel reaction precursor state (**J** in Figures 5 and S10) between the attacking hydrogen and the partially fragmented alkoxy intermediate was identified. Starting from the coadsorption state **G** and a hydrogen atom infinitely far from each other, a coadsorption state (**H**) between a bridge hydrogen in the direction of the H_d position (Scheme 2) and **G** was first

formed. The subsequent activation barrier (**I**) for forming the precursor state (**J**) was small, 6 kJ mol^{-1}, which is comparable with the energy of hydrogen diffusion on a clean surface.

The consequent hydrogen attack from the atop position (**J**) to carbonyl oxygen (**L**) occurred as a single step and was accompanied by a simultaneous bond formation between carbonyl carbon and the other hydrogen atom at the atop site below the carbonyl carbon (Figure S14). This process was exothermic by 23 kJ mol^{-1} and had a moderate activation energy barrier of 45 kJ mol^{-1} (**K**). Desorption of the adsorbed product diol (**L**) to the gas-phase diol (**M**) was endothermic by 128 kJ mol^{-1}. The whole reaction from the gas-phase reactants to the gas-phase product (1*R*,2*R*)-diol was exothermic by 69 kJ mol^{-1}.

To the best of our knowledge, the pairwise addition of hydrogen to the carbonyl group has not been investigated computationally before. Other theoretical studies have considered stepwise mechanisms.[42−48] Kinetic studies of the hydrogenation of simple ketones have generally suggested that either the first or the second H addition is the rate-determining step depending on the catalyst and the reaction conditions.[39a,41,51] However, pairwise addition mechanism has been proposed in some cases for ketones[52,53] and benzene and ethylbenzene hydrogenations.[54,55] In addition, it was recently demonstrated by NMR spectroscopy that hydrogen addition to an alkene on supported metal catalysts occurs pairwise to some extent.[56] Our computational results provide a strong support for the pairwise mechanism in heterogeneously catalyzed hydrogenation of the carbonyl group.

As in the case of hydroxyalkyl hydrogenation route, the potential energy profiles for the pairwise *re*- and *si*-face hydrogenation showed some similarity. The first clear difference in the profiles appeared between the thermodynamic stabilities of the coadsorption states (**G**); the *si*-face adsorption mode was more stable than the *re*-face one by 14 kJ mol^{-1}. The stability difference between the two modes was about the same for the precursor state (**J**). Similar results were obtained on Pt_{38} (Table S7). Therefore, on a catalyst metal surface with hydrogen atoms, the surface is expected to be covered mainly by the *si*-(*s-trans*,*180*)-π_S adsorption mode of (*R*)-PAC.

The pairwise hydrogen addition step from the precursor state (**J**) to the adsorbed diol (**L**) was more exothermic and had a lower activation barrier for the *re*-face addition by 4 kJ mol^{-1}. This difference between the *re*- and *si*-face addition steps, if in the limits of computational accuracy, implies a slower reaction on the *si*-face. Therefore, in the case of pairwise hydrogen addition mechanism, the formation of (1*R*,2*S*)-diol was strongly favored by thermodynamics (more stable adsorption) but slightly disfavored by kinetics (slower hydrogenation of the precursor state).

According to the DFT calculations, all mechanisms considered for (*R*)-PAC hydrogenation on Pt(111) lead to the diastereomeric excess of (1*R*,2*S*)-diol. The adsorption of (*R*)-PAC with coadsorbed hydrogen was clearly more stable through the *si*-face. The activation barriers for hydrogen addition to the *si*-face were lower for the hydroxyalkyl and alkoxy hydrogenation routes and only slightly higher for the pairwise hydrogenation.

Table 3. Activation Energy Difference (ΔE_a) and Reaction Energy Difference ($\Delta\Delta E_r$) between *re*- and *si*-Face Hydrogen Attacks for Various Elementary Steps of (*R*)-PAC Hydrogenation on Pt(111)[a]

elementary step	ΔE_a[b]	$\Delta\Delta E_r$[b]
hydroxyalkyl route, first step (**H** → **J**)[c]	1	0
hydroxyalkyl route, second step (**K** → **M**)[c]	13	−2
alkoxy route, first step (**G** → alkoxy)[d]	4	9
pairwise route (**J** → **L**)[d]	−4	−4

[a] Energies in kJ mol^{-1}. [b] The energy difference has been obtained by subtracting the energy for the *si*-face attack from that for the *re*-face attack. [c] See Figure 4 and Table S3 for the acronyms. [d] See Figure 5 and Table S4 for the acronyms.

The alkoxy hydrogenation route was unfavorable due to the very low stability of the alkoxy intermediate. On the other hand, the formation of the hydroxyalkyl intermediate was exothermic. However, the second elementary hydrogen addition step of the hydroxyalkyl hydrogenation route had quite a high activation energy barrier (over 100 kJ mol^{-1}), whereas the pairwise hydrogen addition step had a moderate activation barrier (less than 50 kJ mol^{-1}). The pairwise addition mechanism corresponds to the minimum energy pathway from adsorbed reactants to adsorbed products and could be the main mechanism for (*R*)-PAC hydrogenation on Pt(111).

Finally, an important observation about the energy profiles for (*R*)-PAC hydrogenation (Figures 4 and 5) was made. A qualitative relation between the reaction energies of the elementary hydrogen addition steps and the corresponding activation energies existed (Table 3). If the reaction energies for hydrogen addition were equal on both diastereotopic faces ($\Delta\Delta E_r \approx 0$), so were the activation energies ($\Delta E_a \approx 0$), as exemplified by the first step of hydroxyalkyl hydrogenation route. If the elementary step was more exothermic on the *re*-face ($\Delta\Delta E_r < 0$), the activation energy was lower for the *re*-face addition ($\Delta E_a < 0$). More generally, if the hydrogen addition step was thermodynamically more favorable on one of the two diastereotopic faces, it was also kinetically preferred on the same face, and vice versa. The only step that seemed not to follow this relation was the second hydrogenation step of the hydroxyalkyl route. The relation suggests that qualitatively correct estimations regarding the sense and degree of diastereoselectivity may be made on the basis of the thermodynamic stabilities of surface intermediates.

3.3. Hydrogenation of Other Chiral α-Hydroxyketones on Pt(111). Experimental studies on some chiral α-hydroxyketones besides (*R*)-PAC have shown that hydrogenation of (*R*)-3-hydroxy-2-butanone [(*R*)-acetoin henceforward] on Pt/Al_2O_3 yields 14% diastereomeric excess of (2*R*,3*R*)-butane-2,3-diol over (2*S*,3*R*)-*meso*-butane-2,3-diol,[57] whereas hydrogenation of (*R*)-2-hydroxy-1-cyclohexanone [(*R*)-adipoin henceforward] on Pt/Al_2O_3 yields 29% de of (1*S*,2*R*)-*meso*-cyclohexane-1,2-diol over (1*R*,2*R*)-cyclohexane-1,2-diol[58] (Scheme 4). As hydrogenation of (*R*)-PAC on Pt/Al_2O_3 gives 49% de of (1*R*,2*S*)-diol, these two other chiral α-hydroxyketones offer a good opportunity to further elucidate the origin of diastereoselectivity and to assess the validity of our theoretical model in predicting the de.

The same strategy as with (*R*)-PAC was applied to study (*R*)-acetoin and (*R*)-adipoin hydrogenation. However, because

(51) Lemcoff, N. O. *J. Catal.* **1977**, *46*, 356.
(52) Chang, N.-S.; Aldrett, S.; Holtzapple, M. T.; Davison, R. R. *Chem. Eng. Sci.* **2000**, *55*, 5721.
(53) Gao, F.; Allian, A. D.; Zhang, H.; Cheng, S.; Garland, M. *J. Catal.* **2006**, *241*, 189.
(54) Temkin, M. I.; Murzin, D. Yu.; Kul'kova, N. V. *Kinet. Katal.* **1989**, *30*, 637.
(55) Smeds, S.; Murzin, D.; Salmi, T. *Appl. Catal., A: Gen.* **1995**, *125*, 271.
(56) Kovtunov, K. V.; Irene, E. B.; Bukhtiyarov, V. I.; Koptyug, I. V. *Angew. Chem., Int. Ed.* **2008**, *47*, 1492.
(57) Studer, M.; Okafor, V.; Blaser, H.-U. *Chem. Commun.* **1998**, 1053.
(58) Sonderegger, O. J.; Bürgi, T.; Baiker, A. *J. Catal.* **2003**, *215*, 116.

Scheme 4. Hydrogenation of (*R*)-Acetoin Yields 14% de of (2*R*,3*R*)-Butane-2,3-diol, Whereas Hydrogenation of (*R*)-Adipoin Gives 29% de of *meso*-Cyclohexane-1,2-diol over Pt/Al_2O_3[a]

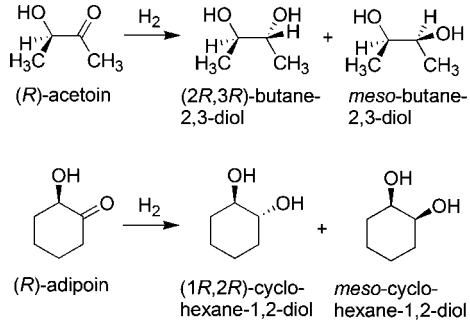

[a] The de's have been calculated from the rate constants given in refs 57 and 58.

searching for transition states is computationally very demanding, only stable species of the hydrogenation reaction were considered. The catalyst surface was modeled by the two-layer Pt_{31} cluster, and the calculations were performed at the BP86/SVP–MARI-*J* level of theory.

3.3.1. Thermodynamic Stabilities of the Products. The most stable gas-phase product diols from (*R*)-acetoin and (*R*)-adipoin hydrogenation had an intramolecular OH···OH hydrogen bond (Figure S15). (*R*,*R*)-Diol was slightly more stable than its diastereomer (by 2−4 kJ mol^{-1}), just as in the case of the hydrogenation products of (*R*)-PAC. In the absence of activation energy barriers or at equilibrium conditions, these results would imply an excess formation of (*R*,*R*)-diol. The experimental de of (*R*)-adipoin hydrogenation does not directly correlate with the thermodynamic stabilities of the products.

3.3.2. Adsorption on Pt(111). The difference between the molecular structures of (*R*)-acetoin and (*R*)-PAC is the substituent attached to the $CH_3C(O)CHOH$ framework: in (*R*)-PAC it is the phenyl moiety, whereas in (*R*)-acetoin it is the methyl group. As in the case of (*R*)-PAC, the minimum energy gas-phase conformation of (*R*)-acetoin had an internal C═O···HO hydrogen bond with the O═C−C−OH moiety being planar. In contrast to (*R*)-PAC whose adsorption was complicated by the phenyl ring, (*R*)-acetoin can be adsorbed with less possible variations. Six different adsorption modes of (*R*)-acetoin leading to both (*R*,*R*)- and *meso*-diols were considered by DFT (Tables 4 and S5, Figures 6 and S16). The *re*-(*s-cis*) mode (ΔE_{ads} = −41 kJ mol^{-1}) was the most stable *re*-face adsorption mode of (*R*)-acetoin as it was for (*R*)-PAC. Instead, the most stable *si*-face adsorption mode of (*R*)-acetoin was not *si*-(*s-trans*,*180*) but *si*-(*s-cis*) with an adsorption energy of −43 kJ mol^{-1}. This can be explained by the formation of an intramolecular C═O···HO hydrogen bond in *si*-(*s-cis*).

In general, (*R*)-acetoin adsorbed more weakly than (*R*)-PAC on Pt(111); the adsorption energy differences between corresponding adsorption modes of (*R*)-PAC and (*R*)-acetoin were up to ca. 120 kJ mol^{-1}. Obviously, this fact can be attributed to the high adsorption energy of the phenyl ring of (*R*)-PAC. On the other hand, the adsorption energies of such adsorption modes where the phenyl/methyl groups were not directly adsorbed were quite close to each other.

The molecular structure of (*R*)-adipoin may be considered as a cyclic congener of (*R*)-acetoin (Scheme 4). The cyclic structure reduces the number of possible adsorption modes because the (O)C−C(OH) bond cannot rotate as readily as in acyclic α-hydroxyketones. Only chair conformations of the six-membered ring were considered here because α-substituted cyclohexanones exist in two stable chair conformations.[59] The OH group in these two conformations may adopt an axial or equatorial position. The O═C−C−OH moiety in the equatorial conformer was planar and had an intramolecular hydrogen bond. Such a stabilizing interaction was not conceivable for the axial conformer, which was reflected in its 22 kJ mol^{-1} lower thermodynamic stability.

Table 4. Adsorption Energy (ΔE_{ads}), Sum of π and π^* Orbital Energies (ΔE_{orb} for α Spin; for β Spin Essentially the Same Energies) Relative to the Most Stable Orbitals, and Bond Distances and Torsion Angles for Different Adsorption Modes of (*R*)-Acetoin and (*R*)-Adipoin on the (111) Surface of a Relaxed Pt_{31} Cluster Calculated at the BP86/SV(P) Level of Theory[a]

adsorption mode	ΔE_{ads} (kJ mol^{-1})	ΔE_{orb} (kJ mol^{-1})	C═O (pm)	φ (deg)[b]
(*R*)-Acetoin				
re-(*s-cis*)	−41	1	136	123
re-(*ortho*,*180*)	+10		134	133
re-(*s-trans*,−*60*)	−31		134	133
si-(*ortho*,−*60*)	−17		137	−125
si-(*s-cis*)	−43	5	136	−127
si-(*s-trans*,*180*)	−12	0	134	−131
(*R*)-Adipoin				
re-(*s-trans*,−*60*)	−32	1	135	127
re-(*s-cis*)	−45	57	135	125
si-(*ortho*,−*60*)	−15	0	136	−125
si-(*s-cis*)	−52	30	136	−127

[a] More details of the adsorption modes can be found in Table S5. [b] This torsion angle corresponds to the one reported for (*R*)-PAC in Table 2. It indicates distortion of the C−CO−C moiety from planarity: $|\varphi| = 180° \Rightarrow$ planar; $|\varphi| = 120° \Rightarrow$ tetrahedral.

Two axial and two equatorial adsorption modes of (*R*)-adipoin leading to both (*R*,*R*)- and *meso*-diols were considered by DFT (Tables 4 and S5, Figures 6 and S17). As expected on the basis of the gas-phase results, the equatorial conformations *re*-(*s-cis*) and *si*-(*s-cis*) with adsorption energies of −45 and −52 kJ mol^{-1}, respectively, were clearly more stable than the axial ones even on the surface. Thus, geometries of the most stable *re*- and *si*-face adsorption modes of (*R*)-acetoin and (*R*)-adipoin were similar to each other; all of them had an intramolecular OH···O═C hydrogen bond.

In general, adsorption of (*R*)-adipoin on Pt was slightly stronger than adsorption of (*R*)-acetoin (Table 4). Adsorption by the *si*-face was the most thermodynamically favorable for both compounds. The stability difference between the *si*-(*s-cis*) and *re*-(*s-cis*) adsorption modes was 7 kJ mol^{-1} for (*R*)-adipoin and 2 kJ mol^{-1} for (*R*)-acetoin. Therefore, (*R*)-adipoin will predominantly be adsorbed through its *si*-face on the Pt(111) surface, whereas the populations of *re*- and *si*-face adsorbed (*R*)-acetoin will be almost equal. The results of analyzing the carbonyl π and π^* orbitals implied that addition of hydrogen proceeds more rapidly to the *si*-(*s-cis*) than the *re*-(*s-cis*) mode of (*R*)-adipoin. In the case of (*R*)-acetoin, hydrogenation of the *re*-face was more favored due to the lower energies of the carbonyl orbitals.

3.3.3. Hydrogenation. The first hydrogen attack to the carbonyl oxygen yielding the hydroxyalkyl intermediate was an exothermic reaction by 33−34 kJ mol^{-1} for (*R*)-adipoin and by 28−29 kJ mol^{-1} for (*R*)-acetoin (see Table 5 and Figures S18 and S19). The *si*-face hydroxyalkyl intermediates of both (*R*)-adipoin and (*R*)-acetoin were more stable than their *re*-face counterparts by 7 and 2 kJ mol^{-1}, respectively. The second

(59) Basso, E. A. *J. Org. Chem.* **1993**, *58*, 7865.

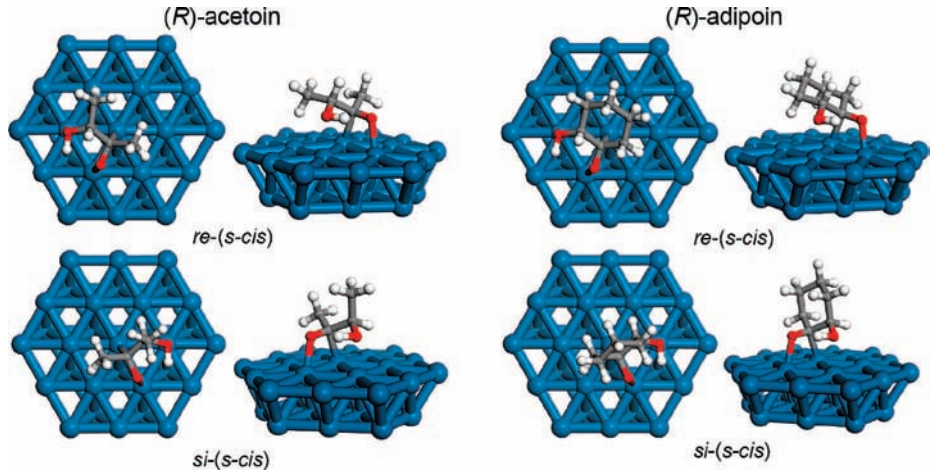

Figure 6. Top and side views of the most stable *re*- and *si*-face adsorption modes of (*R*)-acetoin and (*R*)-adipoin on the Pt_{31} cluster. The structures were optimized at the BP86/SVP level of theory.

Table 5. DFT (BP86/SVP) Computed Energies of Various Stable Species in the Hydrogenation of (*R*)-PAC, (*R*)-Adipoin, and (*R*)-Acetoin on Pt(111) Involving the Hydroxyalkyl and Alkoxy Intermediates of the Stepwise Mechanisms as well as the Precursor State of the Pairwise Mechanism[a]

species	(*R*)-PAC	(*R*)-adipoin	(*R*)-acetoin
reactant* + 2H*			
re-face	−208	−150	−148
si-face	−213	−156	−149
hydroxyalkyl intermediate* + H*			
re-face	−238	−183	−176
si-face	−254	−190	−178
alkoxy intermediate* + H*			
re-face	−105	−106	−106
si-face	−128	−101	−98
precursor state*[b]			
re-face	−174	−128	−131
si-face	−189	−128	−129
product diol*			
(*R*,*R*)	−197	−158	−155
(*R*,*S*)	−208	−151	−147
product diol(g)			
(*R*,*R*)	−69	−69	−67
(*R*,*S*)	−66	−67	−64

[a] Energies are relative to the reference state (most stable gas-phase reactant, gas-phase H_2, and bare Pt_{31} cluster). The more negative is the energy, the more stable are the species. [b] Precursor state in the pairwise addition mechanism, that is, a coadsorption state between adsorbed reactant and two hydrogen atoms that precedes immediately the adsorbed product diol.

hydrogen attack to the carbon was endothermic by 25−39 kJ mol^{-1} for (*R*)-adipoin and by 21−31 kJ mol^{-1} for (*R*)-acetoin. The reaction energies were of similar magnitude for (*R*)-PAC and other carbonyl compounds considered above.[43−45,47,48]

The reaction step from the adsorbed reactants to the alkoxy intermediate was endothermic by 40−55 kJ mol^{-1} for (*R*)-adipoin and (*R*)-acetoin (Table 5). This reaction energy is in agreement with the previously reported values for carbonyl compounds[23,43−45,47,48] but is almost 50 kJ mol^{-1} less than for (*R*)-PAC. It is very likely that the chemisorbed phenyl ring of (*R*)-PAC hindered the alkoxy intermediate from adopting a more stable geometry. The *re*-face alkoxy intermediates of both (*R*)-adipoin and (*R*)-acetoin were more stable than their *si*-face counterparts by 5 and 8 kJ mol^{-1}, respectively. The second hydrogen attack to the oxygen was exothermic by 49−52 kJ mol^{-1}, which is of similar magnitude as found previously.[23,43,45,47,48]

The reaction step from adsorbed reactants to the precursor state of the pairwise mechanism was endothermic by 22−28 kJ mol^{-1} for (*R*)-adipoin and by 17−20 kJ mol^{-1} for (*R*)-acetoin (Table 5). For (*R*)-PAC, this step was slightly more endothermic, by 24−34 kJ mol^{-1}. The *re*- and *si*-face precursor states of (*R*)-adipoin were of equal stability, whereas the *re*-face precursor state of (*R*)-acetoin was more stable than its *si*-face counterpart by 2 kJ mol^{-1}.

Adsorbed (*R*,*R*)-diastereomers of cyclohexane-1,2-diol and butane-2,3-diol were more stable than their (*R*,*S*)-diastereomers (*meso*-diols) by 7−8 kJ mol^{-1}, whereas (1*R*,2*S*)-diol was the more stable product diastereomer of (*R*)-PAC hydrogenation. Desorption from the Pt(111) surface was endothermic by 80−90 kJ mol^{-1} for cyclohexane-1,2-diol and butane-2,3-diol and required 5 kJ mol^{-1} more energy for (*R*,*R*)-diol than *meso*-diol.

3.4. Comparison of Computational and Experimental Data. The experimentally observed diastereoselectivity in chiral α-hydroxyketone hydrogenation over Pt is a result of several elementary steps of reaction, including adsorption and surface reaction. The picture can be complicated if several feasible surface adsorption modes and reaction mechanisms exist. No quantitative values for the de were derived from the DFT results because information about pre-exponential factors would be needed to get accurate values for the formation rates of the diastereomeric product diols.[60] This in turn would require calculating the vibrational frequencies of the adsorbed species, which was computationally too demanding for molecules in the present study. For the same reason, effects of zero-point energies on binding energies and activation energy barriers were not considered in this study. Although these effects are not negligible, they probably do not alter the qualitative trends in the reaction network described above.[43]

Figure 7 shows relative thermodynamic stabilities of various *re*- and *si*-face adsorbed species in the hydrogenation of (*R*)-PAC, (*R*)-adipoin, and (*R*)-acetoin, and the corresponding values for experimentally observed diastereomeric excesses of the (*R*,*S*) product diol (49%, 29%, and −14%, respectively). If ΔE is positive, the *si*-face adsorbed species or (*R*,*S*)-diol is more stable; if ΔE is negative, the *re*-face adsorbed species or (*R*,*R*)-diol is more stable. The *si*-face adsorbed (*R*)-PAC and its hydrogena-

(60) For prediction of experimental reaction rates from first principles, see, for example: Kandoi, S.; Greeley, J.; Sanchez-Castillo, M. A.; Evans, S. T.; Gokhale, A. A.; Dumesic, J. A.; Mavrikakis, M. *Top. Catal.* **2006**, *37*, 17.

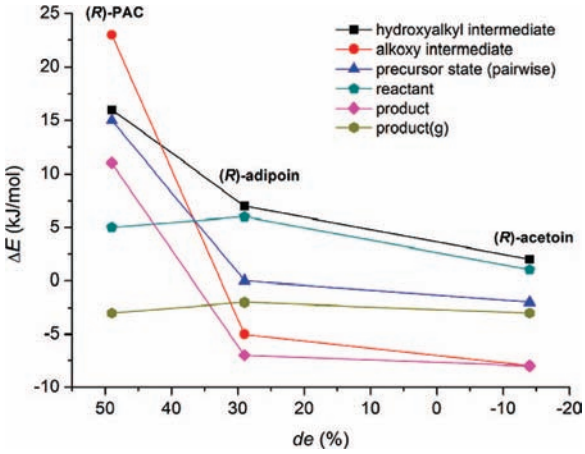

Figure 7. Relative energies of *re*- and *si*-face adsorbed species versus experimentally observed diastereomeric excess for the hydrogenation of (*R*)-PAC (de = 49%), (*R*)-adipoin (29%),[58] and (*R*)-acetoin (−14%).[57] For reactants, intermediates, and precursor states, ΔE is defined as E(*re*-face) − E(*si*-face); for hydrogenation products, $\Delta E = E$[(*R*,*R*)-diol] − E[(*R*,*S*)-diol]; de (%) = 100 × [(*R*,*S*) − (*R*,*R*)]/[(*R*,*S*) + (*R*,*R*)]. All species other than "product(g)" are adsorbed on the Pt(111) surface. Potential energies of all species are given in Table 5.

tion intermediates were more stable than their *re*-face adsorbed congeners by 5−25 kJ mol^{-1}. The adsorbed (1*R*,2*S*)-diol was also more stable than (1*R*,2*R*)-diol. As was discussed above, this implies an excess formation of (1*R*,2*S*)-diol. When moving from (*R*)-PAC to (*R*)-adipoin and further to (*R*)-acetoin (from left to right in Figure 7), the ΔE values for various reaction species decreased as a rule. That is, the stability difference between the *re*- and *si*-face species in favor of *si*-face was less pronounced for (*R*)-adipoin and even smaller for (*R*)-acetoin. This suggests a decrease in the de, thus being well in line with the experimental data. The *re*- and *si*-face adsorbed reactants and hydroxyalkyl intermediates of (*R*)-acetoin were almost equally stable, whereas the alkoxy intermediate and the precursor state of the pairwise mechanism were more stable when adsorbed through their *re*-face. (*R*,*R*)-Diol was also more stable than *meso*-diol. These results are consistent with the small de of (2*R*,3*R*)-butane-2,3-diol.

4. Summary and Conclusions

Hydrogenation of (*R*)-1-hydroxy-1-phenyl-2-propanone [(*R*)-PAC] was studied in this work by both experimental and theoretical approaches. When this chiral α-hydroxyketone was hydrogenated in toluene over Pt/Al_2O_3 in the absence of any modifier, (1*R*,2*S*)-1-phenyl-1,2-propanediol was formed in excess (de = 49%) over its diastereomer, (1*R*,2*R*)-1-phenyl-1,2-propanediol. In the presence of the cinchonidine modifier, the diastereomeric excess increased to ca. 60%. In acetic acid, hydrogenation of (*R*)-PAC proceeded at an extremely low rate.

As the first step to rationalize the observed diastereomeric excess, the thermodynamic stabilities of the diastereomeric gas-phase product diols were determined using density functional theory (DFT) calculations. The stabilities of the products were not directly proportional to the observed product ratio. Adsorption of (*R*)-PAC on Pt(111) was then investigated using cluster model DFT calculations. Twenty-five different adsorption modes were optimized. The phenyl and carbonyl moieties were chemisorbed parallel to the surface in the most stable adsorption modes. Hydrogen bonding between the hydroxyl hydrogen and the carbonyl oxygen (or the Pt surface) had a stabilizing effect. Adsorption energies of the most stable *re*- and *si*-face adsorbed species were of similar magnitude, ca. −130 kJ mol^{-1} on the Pt_{38} cluster. The analysis of the bonding π and antibonding π^* carbonyl orbitals suggested that the *si*-face adsorbed species undergoes faster hydrogenation due to the more pronounced orbital stabilization.

To further reveal the origin of diastereodifferentiation in (*R*)-PAC hydrogenation, full potential energy profiles (including stable intermediates and transition states) for various hydrogenation pathways on the Pt(111) surface were determined by DFT. The activation energy barriers were lower for hydrogen attacks that took place at the C═O moieties partially decoordinated from the surface. Formation of the C−H bonds was endothermic, whereas formation of the O−H bonds was exothermic.

The hydroxyalkyl hydrogenation route, where a hydrogen atom attacks the carbonyl oxygen first, had a high (over 100 kJ mol^{-1}) activation energy barrier for the second hydrogen attack at the carbon atom. Therefore, the thermodynamically quite stable hydroxyalkyl intermediate is more likely to be decomposed into (*R*)-PAC and hydrogen than to be hydrogenated further to the product diol. On the other hand, the alkoxy hydrogenation route was associated with a high (ca. 100 kJ mol^{-1}) activation barrier for the first formation of the C−H bond. The alkoxy intermediate was thermodynamically very unstable and had a low barrier (1−6 kJ mol^{-1}) for the backward dehydrogenation step. In addition, the reaction energy was close to the desorption energy of (*R*)-PAC. Therefore, formation of the alkoxy intermediate is unlikely. The pairwise hydrogenation route, where two hydrogen atoms attacked the decoordinated carbonyl carbon and oxygen atoms simultaneously, was found to have a reasonable activation barrier (ca. 50 kJ mol^{-1}) for the hydrogen addition step. Therefore, it corresponds to the minimum energy pathway from the adsorbed reactants to the adsorbed products and is proposed to be the main mechanism for (*R*)-PAC hydrogenation on Pt(111).

The DFT calculations suggested that all mechanisms considered for (*R*)-PAC hydrogenation on Pt(111) led to the diastereomeric excess of (1*R*,2*S*)-diol. The diastereodifferentiation was a result of both thermodynamic and kinetic factors; the adsorption of (*R*)-PAC with coadsorbed hydrogen was more stable through the *si*-face than the *re*-face, and the activation barriers for hydrogen addition to the *si*-face were nearly equal to or lower than the *re*-face.

Adsorption and hydrogenation of two other chiral α-hydroxyketones, (*R*)-3-hydroxy-2-butanone [(*R*)-acetoin] and (*R*)-2-hydroxy-1-cyclohexanone [(*R*)-adipoin], were also studied on Pt(111) by DFT. The molecular structure had an effect on adsorption energies and the relative stabilities of various adsorption modes, their π and π^* carbonyl orbitals, and the hydrogenation intermediates.

Whereas all the hydrogenation mechanisms implied an excess formation of (1*R*,2*S*)-diol from (*R*)-PAC hydrogenation, the stability difference between the corresponding *re*- and *si*-face adsorbed species in favor of the *si*-face species was less pronounced for (*R*)-adipoin (Figure 7). This suggested a lower de of (*R*,*S*)-diol (*meso*-diol) than for (*R*)-PAC hydrogenation, which is in line with experiments. The *re*- and *si*-face adsorbed reactants and hydroxyalkyl intermediates of (*R*)-acetoin were almost equally stable, whereas the alkoxy intermediate and the precursor state of the pairwise addition mechanism were more stable when adsorbed through their *re*-face. These results imply a nonexistent to small de of (*R*,*R*)-diol and are again consistent with experiments.

The results show that cluster model DFT calculations can be used to assess (dia)stereoselectivity in metal-catalyzed hydrogenation of even such conformationally flexible molecules as studied here, provided that the whole reaction path or at least the stable reaction intermediates are taken into consideration.

Acknowledgment. Professor Michael Müller from the University of Freiburg is gratefully acknowledged for providing (*R*)-1-hydroxy-1-phenyl-2-propanone and for fruitful discussions. This work is part of the activities at the Åbo Akademi Process Chemistry Centre within the Finnish Centre of Excellence Programme (2000−2011) by the Academy of Finland. Computer resources provided by CSC, the Finnish IT center for science, are kindly acknowledged. I.B. is grateful for the postdoctoral fellowship from the Magnus Ehrnrooth Foundation. I.B. carried out the experiments; A.T. performed the computations; and I.B. and A.T. cowrote this Article.

Supporting Information Available: Details of the synthesis of (*R*)-1-hydroxy-1-phenyl-2-propanone, details of (*R*)-PAC adsorption and hydrogenation, details of the effects of adsorption mode orientation and cluster size on adsorption, Tables S1−S8, Schemes S1 and S2, and Figures S1−S19. This material is available free of charge via the Internet at http://pubs.acs.org.

JA809070G